Editors' Suggestion

Gate-voltage switching of nonreciprocal transport in oxide-based Rashba interfaces

Julien Bréhin[1,†] Luis M. Vicente Arche,[1] Sara Varotto,[1] Srijani Mallik,[1] Jean-Philippe Attané,[2] Laurent Vila,[2] Agnès Barthélémy,[1] Nicolas Bergeal,[3] and Manuel Bibes[1,*]

[1]*Unité Mixte de Physique, CNRS, Thales, Université Paris-Saclay, Palaiseau, France*

[2]*University Grenoble Alpes, CEA, CNRS, Grenoble INP, SPINTEC, Grenoble 38000, France*

[3]*Laboratoire de Physique et d'Etude des Matériaux, UMR 8213—CNRS, ESPCI-Paris, PSL, Sorbonne Université, Paris, France*

The linear magnetoelectric effect (ME) is the phenomenon by which an electric field produces a magnetization. Its observation requires both time-reversal and space-inversion symmetries to be broken, as in multiferroics. While the ME effect has only been studied in insulating materials, it can actually exist in noncentrosymmetric conductors such as two-dimensional electron gases (2DEGs) with Rashba spin-orbit coupling. It is then coined the Edelstein effect (EE), by which a bias voltage—generating a charge current—produces a transverse spin density, i.e., a magnetization. Interestingly, 2D systems are sensitive to voltage gating, which provides an extra handle to control the EE. Here, we show that the sign of the EE in a $SrTiO_3$ 2DEG can be controlled by a gate voltage. We propose various logic devices harnessing the dual control of the spin density by current and gate voltages and discuss the potential of our findings for gate-tunable nonreciprocal electronics.

I. INTRODUCTION

As classical semiconductor electronics reaches its physical limits and the power consumption of computing architectures increases dramatically [1], alternative paradigms of computation are emerging, notably harnessing the electron's spin in addition to its charge [2]. Realizing beyond-CMOS devices operating on spin requires the implementation of schemes to electrically generate, control, and detect spin-encoded information. Key concepts in this endeavor are the magnetoelectric effect (ME, to generate and control a magnetization by an electric field) and spin-charge interconversion. The latter can be achieved by the direct and inverse spin Hall (SHE) [3] and Edelstein effects (EE) [4]. The SHE directly generates a spin current from a charge current while the inverse SHE (ISHE) does the reciprocal operation. The EE generates a spin density (that is, a magnetization) from a charge current; the spin density can then diffuse in adjacent layers as a spin current. Reciprocally, the inverse EE (IEE) generates a charge current from an injected spin density.

Examples of spin-based logic devices include Intel's MESO transistor [5,6] (in which the ME is used to write

magnetic information and the ISHE or IEE is used to read it out) or the FESO concept [7] (that harnesses the ferroelectric control of the IEE [7] or the ISHE [8,9]).

While the ME [10] and EE [4] look *a priori* quite distinct, the EE may appear as a form of ME arising in conducting systems (the ME is usually restricted to insulating polar magnets such as Cr_2O_3 or multiferroics), as was actually pointed out by Edelstein himself [4]. The EE has been reported in surface states of topological insulators [11] and at Rashba interfaces including Ge(111) [12] and oxide interfaces [13–16]. However, the sign of the EE, determining the direction of the nonequilibrium magnetization generated by the applied charge current, is intrinsic to the band structure of the material and is thus usually fixed.

Here, by injecting an electrical current in an AlO_x/$SrTiO_3$ two-dimensional electron gas (2DEG) patterned into a Hall bar, we demonstrate the generation of a magnetization via the EE, that manifests as an additional longitudinal resistance upon applying a transverse magnetic field. This resistance term depends linearly on the current, indicating that the sign of the EE-generated magnetization changes when switching the current direction. We show that it is possible to also change its sign by applying a gate voltage, which tunes the Fermi energy across the competing Rashba-split electronic band pairs of the $SrTiO_3$ (STO) 2DEG [17,18]. This provides a unique dual control of the

---

EE-generated magnetization, which we propose to exploit in various types of spintronic logic gate devices free from ferromagnets.

II. THEORETICAL BACKGROUND

The Rashba effect [19] results from the coexistence of a broken inversion symmetry—which is typically present at a heterostructure interface and manifests as an electric field perpendicular to that interface—and a sizeable spin-orbit interaction (SOI). The direct consequence is the lifting of spin degeneracy in momentum space, introduced by term $H_R = (\alpha_R/\hbar)(\sigma \times p) \cdot \hat{\mathbf{z}}$ in the Hamiltonian, where $\hbar$ is the reduced Planck constant, $\boldsymbol{\sigma}$ is the vector of Pauli matrices, $\mathbf{p}$ is the electron momentum, and $\hat{\mathbf{z}}$ is a unit vector normal to the plane of the heterointerface (and thus, parallel to the symmetry-breaking electric field) and α_R is a constant that quantifies the strength of the Rashba SOI and the resulting spin splitting. It appears from this term that the spin and momentum degrees of freedom will be locked perpendicular to each other and, in a system where the Rashba splitting occurs near the Fermi level, the Fermi surface will consist of two concentric contours with opposite chirality of the spin winding [20].

In the semiclassical picture of transport, applying an electric field across the 2DEG and thus injecting a charge current $\mathbf{j^c}$ along one direction, say $-\mathbf{x}$, results in a shift of both inner and outer contours by the same amount Δk_x. This generates an excess spin densities δs_+ and δs_- for each contour as seen in Fig. 1(a). Since these two contours do not coincide, these two densities are not equivalent, they do not compensate each other and a finite spin density (a magnetization) transverse (i.e., along the y axis) and proportional to the charge current appears in the system. This magnetoelectric effect converting a charge current into a spin current was first described in Ref. [4] and is referred to as the direct EE or the inverse spin galvanic effect.

It is worthwhile to note that, upon reversal of the sign of the injected charge current, the net magnetization generated will change its orientation accordingly. Thus, an external magnetic field $\mathbf{B}$ applied in plane will interact constructively or destructively with the generated magnetization depending on the sign of the current and the applied field orientation, leading to a decrease or to an increase of the sample resistance. This unidirectional magnetoresistance term then has two extrema as a function of the angle Φ between the current and the field, namely when they are transverse to each other, and it is proportional to both the injected current density and the applied magnetic field. As such, it is also called bilinear magnetoresistance (BMR) and its angular dependence has been found by Vaz *et al.* [14] to follow

$$R_{\text{BMR}} = A_{\text{BMR}} \frac{j_x^c}{j^c} \sin \Phi, \quad (1)$$

where

$$A_{\text{BMR}} = \frac{3}{2}\pi \frac{g\mu_B}{|e|\hbar} \frac{\alpha_R \tau^2}{\epsilon_F} j^c B, \quad (2)$$

in the case where one uses normalized magnetoresistance MR $= [R_s(B) - R_s(B = 0)]/R_s(B = 0)$ and with Φ the angle between the injected charge current $\mathbf{j^c}$ and the applied in-plane magnetic field $\mathbf{B} = \mu_0\mathbf{H}_\parallel$. For a given set of experimental conditions, the amplitude of this effect can thus be used to estimate the Rashba coefficient α_R. However, it is also highly dependent on other physical parameters of the system, such as the scattering time τ, the g factor, and Fermi energy ϵ_F. Of note, in the case of oxide 2DEGs, it is known that these three parameters can vary when applying a gate voltage, in addition to α_R [17,21,22].

Concurrently to the BMR, the magnetoresistance is also modulated by an anisotropic π-periodic term that is independent on the current but that scales quadratically with the
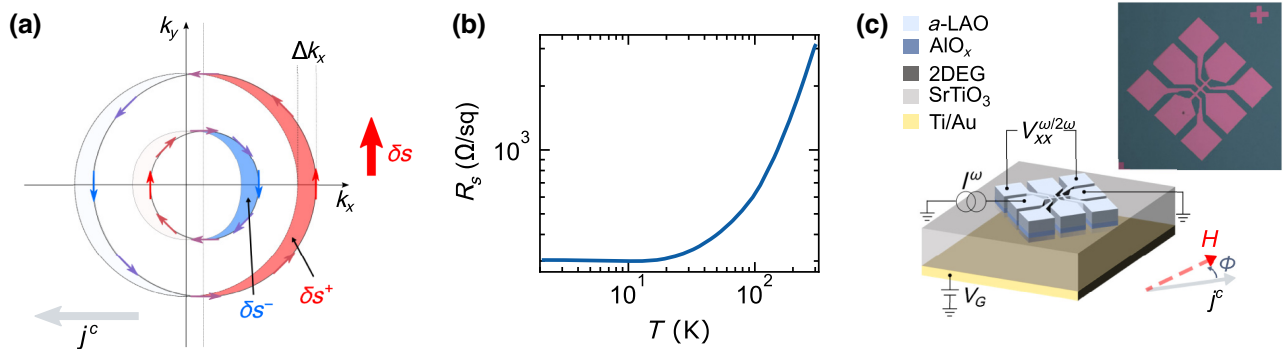

FIG. 1. (a) Fermi contours resulting from the direct Edelstein effect (DEE) in a simple Rashba system with spin-split parabolic bands. Upon injection of a charge current $\mathbf{j^c}$ along $-x$, both Fermi contours are shifted in the same direction by Δk_x, creating a net density of spins with transverse direction, and resulting in a net magnetization. (b) Temperature dependence of the sheet resistance of a device based on *a*-LAO/Al/STO 2DEG (LAO: LaAlO$_3$). (c) Schematic of the sample and measurement configuration used throughout the paper. The inset shows a microscope image of the actual device used hereafter.

applied magnetic field, i.e., a quadratic magnetoresistance (QMR) term [14,23]:

$$R_{QMR} = A_{QMR} \cos 2\Phi, \qquad (3)$$

where

$$A_{QMR} = \frac{3}{4} \left(\frac{g\mu_B}{\hbar} \right)^2 \tau^2 B^2. \qquad (4)$$

Since both the BMR and QMR are increasing with τ^2, taking the ratio between their amplitudes removes one system-dependent variable and simplifies the expression into a function depending mainly on universal constants and fixed experimental parameters:

$$\frac{A_{BMR}}{A_{QMR}} = \frac{2\pi\hbar}{|e|g\mu_B} \frac{\alpha_R}{\epsilon_F} \frac{j^c}{B}. \qquad (5)$$

This model provides an efficient method to extract a Rashba coefficient in different systems, and has been applied already to LAO/STO and KTaO$_3$ 2DEGs, yielding values consistent with the literature [21,24,25]. In LAO/STO, Vaz *et al.* have shown a gate-induced modulation by a factor approximately 2.5 of the Rashba coefficient extracted from the BMR [14]. In the next section, we show results for AlO$_x$/STO 2DEGs with a carrier density typically higher than in LAO/STO [26] and evidence a change of sign of the BMR and thus of the effective α_R by a gate voltage.

III. EXPERIMENTAL DETAILS

A. Sample preparation

To characterize the charge-to-spin current conversion, we have performed transport measurements in a 2DEG formed by depositing 2 nm of Al on a STO substrate [26]. We fabricated Hall bar devices via a single-step liftoff process by exposing the design with the SmartPrint projection lithography setup after spin coating a SPR 700 1.0 photoresist on the bare substrate. Al was deposited at room temperature by dc magnetron sputtering on as-received STO (001) substrates from SurfaceNet. During Al deposition, the Ar partial pressure and the dc power were kept fixed at 5.2×10^{-4} mbar and 11 W, respectively, so that the deposition rate was with a rate of approximately 1 Å/s.

The Al in contact with the STO substrate oxidizes into AlO$_x$, which reduces the STO and dopes its surface with electrons, forming the 2DEG [26]. To help increasing the visibility of the devices, a layer of 20 nm of amorphous LaAlO$_3$ (*a*-LAO) was then deposited *ex situ* by PLD at room temperature with a KrF Excimer laser at an energy of 42 mJ, before proceeding to the liftoff with acetone.

B. Magnetotransport measurements

The samples were bonded with Al wire after the patterning process and inserted in a Quantum Design PPMS to measure their transport properties. They show the usual metallic behavior typical of AlO$_x$/STO 2DEGs, with a residual resistivity ratio of approximately 10 between 300 and 2 K, as seen in Fig. 1(b).

At the lowest temperature of 2 K, a back-gate forming step was applied: the gate voltage was first increased to its maximum value $V_{G,max}$ and then cycled repeatedly within the gate range of the experiment $[-V_{G,max}; +V_{G,max}]$ to suppress hysteresis and ensure the full reversibility of the measurements. Figures 2 and 3 were obtained from two distinct cooldowns, with $V_{G,max} = +200$ V and $V_{G,max} = +150$ V, respectively.

The magnetotransport measurements were then performed by rotating the sample under an in-plane constant magnetic field while injecting an alternating current along the main channel of the device and measuring the longitudinal voltage using Stanford Research 830 lock-in amplifiers combined with a Keithley 6221 current source and a Keithley 2400 to apply a gate voltage. With this technique, any resistance oscillation that is linearly dependent on the current amplitude (or more broadly any voltage signal with a quadratic current dependence) will appear in the second harmonic (i.e., at twice the frequency of the injected alternating current, 2ω). In contrast, symmetric terms independent of the current should be found in the first harmonic, ω.

IV. RESULTS

Figure 2(a) shows the angular dependence of the sheet resistance of the device obtained from the first harmonic and normalized by the sheet resistance measured at $B = 0$ T, and for a gate voltage of $V_g = 200$ V. Following the model from Vaz *et al.* [14], the data can be fitted with a cosine of 2Φ as in Eq. (3). The amplitudes A_{QMR} obtained from such fits follow a quadratic dependence with the applied magnetic field as seen in Fig. 2(b).

Using Eq. (4) and assuming the g factor to be equal to 2 as was reported in LAO/STO at high gate voltages [21], we obtain a momentum relaxation time $\tau_m \approx 1.6 \times 10^{-14}$ s, which goes up to 6.4×10^{-14} s for $g = 0.5$ (as used in Ref. [14]). This is in the range of values obtained from a classical transport model with magnetotransport data obtained in the same sample (see Fig. S1 within the Supplemental Material [27]), with $\tau_m \approx 5.5 \times 10^{-14}$ s to 1.2×10^{-13} s at the highest gate voltage (for a d_{xy}-only mass $m^* = 0.6 m_e$ [17] or an estimated $m^* = 1.3 m_e$ used in Ref. [14], respectively).

In addition, as expected from the Edelstein effect, we obtain a 2π-periodic signal from the second-harmonic signal [Figs. 2(c) and 2(e)], which we fit to extract the amplitude and plot as a function of the magnetic field
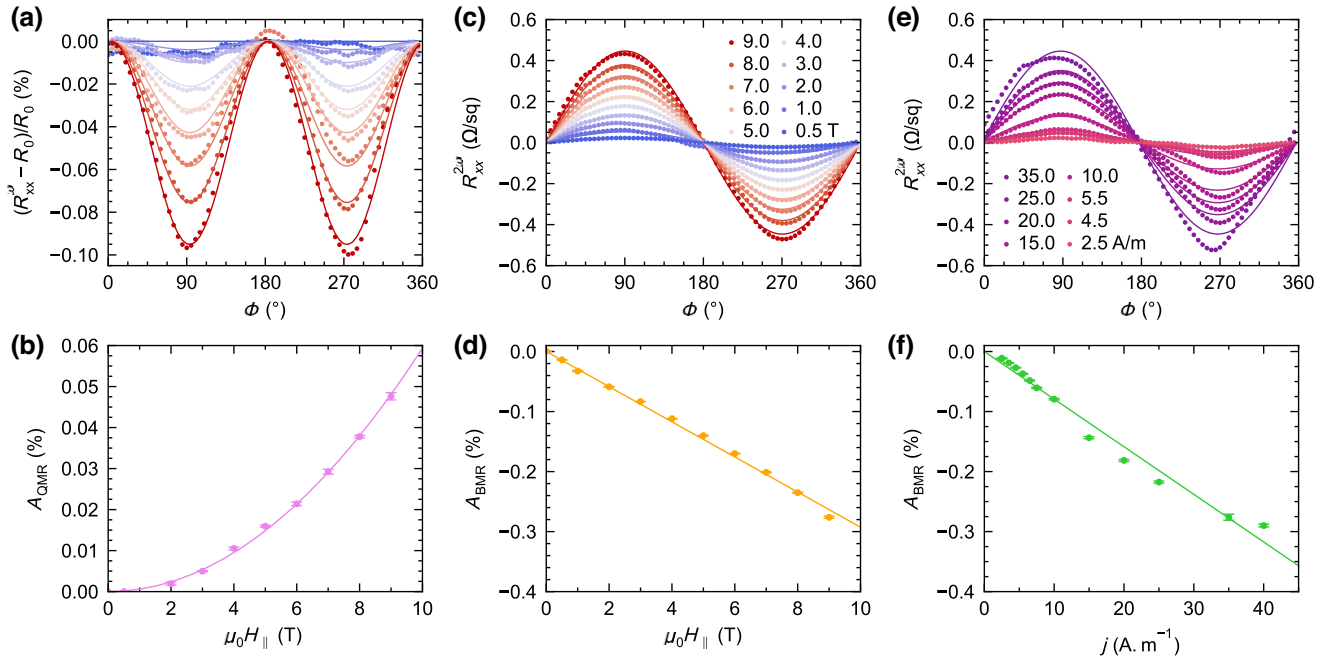
FIG. 2.   Angle dependence of the longitudinal resistance obtained by harmonic transport with an in-plane magnetic field, at a temperature $T = 2$ K and gate voltage $V_g = 200$ V. (a) First-harmonic signal normalized by the (zero-field) sheet resistance $R_0 = R_s(B = 0)$, for magnetic fields at 0.5 T (in blue) and increasing from 2 T up to 9 T (in red) with steps of 1 T. Continuous lines are fits to the experimental data (filled circles). (b) Fitted amplitudes of the first harmonic resistance signal showing a quadratic dependence with the in-plane magnetic field amplitude $\mu_0 H_\parallel$. (c),(e) Angular dependences of the second-harmonic signal $R_{xx}^{2\omega}$ at different fields (c) and current densities (e), showing unidirectional 2π-periodic magnetoresistance. (d),(f) display the corresponding fits of their amplitude as a function of field and current, respectively. Some points on (f) at low current densities correspond to curves not shown on (e) for clarity.

in Fig. 2(d) and as a function of the current density in Fig. 2(f). We see that this signal is mostly linear in both current density and magnetic field, hence it corresponds to the BMR term from charge-to-spin conversion. Note that here, we chose to use the same sign convention as in Ref. [14] where a negative sine function is associated to a positive amplitude and as a consequence, the positive sine function obtained at a gate voltage of 200 V yields a negative BMR amplitude.

Since the Rashba spin-orbit properties of STO 2DEGs are known to vary significantly when applying a gate voltage [14,17,21,22], we have also performed similar measurements at different back-gate voltages, as shown in Fig. 3.

Figure 3(a) shows the second-harmonic signal measured at different gate voltages varying from +125 to −150 V. It is clear that the amplitude of the BMR signal changes significantly and even switches sign, passing from positive to negative amplitude as the gate voltage is increased. The full dependence of A_{BMR} is summarized in Fig. 3(b) where we can identify the crossover to be around $V_g \approx 0$ V to 20 V. We also measured this second-harmonic signal at a fixed angle $\Phi = 90°$, i.e., keeping the current and field perpendicular to each other, while sweeping the magnetic field. Figure 3(c)

confirms the linear dependence of the BMR with the field with opposite slope between $V_g = −100$ V and +75 V.

Checking upon Eq. (2), we see that the BMR amplitude may depend on different system parameters, which can be affected under the application of a back-gate voltage V_g. First, variations of the g factor have been reported from 0.5 to 2.5 in LAO/STO 2DEGs as V_g is increased towards positive values [21]. Yet, this variation cannot explain the sign change of the BMR. In the simple parabolic band model used in Ref. [14], A_{BMR} is also inversely proportional to the Fermi energy and should thus decrease in amplitude as the carrier density is increased but should remain positive. Finally, even considering the quadratic dependence of A_{BMR} with the momentum relaxation time τ, and an increase of the overall mobility as the second type of carrier (from d_{xz}/d_{yz} sub-bands) arises, one could explain the fast increase of the BMR amplitude in absolute value but not the sign change.

In fact, it has been shown previously that the complex band structure of STO 2DEGs with topologically trivial and nontrivial avoided crossings and opposite contributions to the Edelstein tensor between the different sub-bands with d_{xy} and d_{xz}/d_{yz} character could give rise to varying amplitude and sign of the effective Rashba
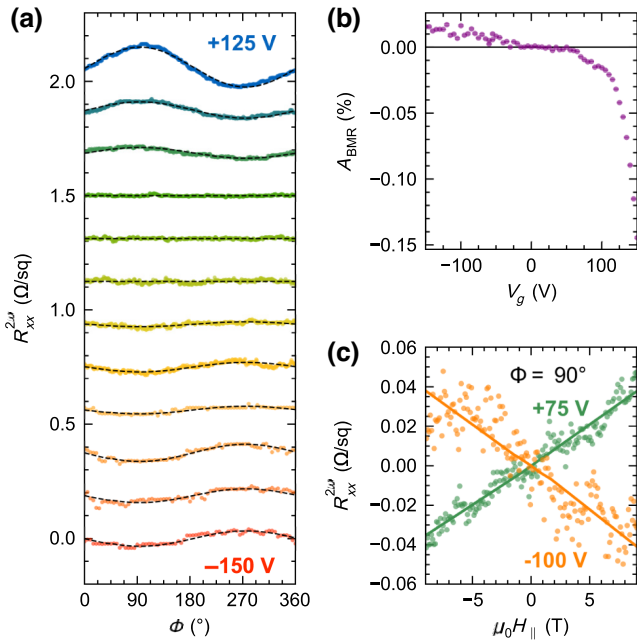
FIG. 3. Gate dependence of the bilinear magnetoresistance obtained from second-harmonic transport measurements with $I_{ac} = 150 \, \mu A$, at a temperature $T = 2$ K. (a) Angle dependence of the second-harmonic signal at fixed gate voltages from -150 to $+125$ V, applying 9 T in the plane of the sample. Circles represent the measured data, after removing some background contributions (see Methods), while the fits are indicated by black dashed lines. Only a few curves are displayed at gate voltages separated by 25 V for the sake of clarity. (b) BMR amplitude extracted from the fits to the angular dependences as a function of the gate voltage. (c) Sheet resistance from the second-harmonic channel as the in-plane magnetic field is swept between $+9$ and -9 T, at $V_g = -100$ V (in orange) and $+75$ V (in green). The lines are a guide to the eye.

coefficient α_R and resulting charge-spin interconversion [14,17,18,28].

Thus, the sign change observed in the BMR signals upon varying the applied voltage most likely reflects a change of α_R as the gate voltage tunes the chemical potential of the system, populating higher states in the band structure with $d_{xz,yz}$ character and opposite Rashba spin texture to that of d_{xy} lower-energy states.

More quantitatively, in the explored gate range and using $g = 0.5$, within the model of Ref. [14] the value of α_R varies from approximately 50 meV Å at large negative voltage to approximately -200 meV Å at large positive voltage. This former value is in the range of what was found in previous reports [21]. However, -200 meV Å clearly exceeds what is expected for STO 2DEGs. Using g factor values of two reported at high carrier densities [21] would make this value even larger, signaling the limits of the model with single parabolic Rashba bands in this case. Overall, these results thus point to the need for developing more elaborate models to compute the BMR from the

band structure, beyond the simple one-band scenario from Ref. [14], i.e., models able to capture better the physics of this system when three or four band pairs are occupied, with a complex electronic structure involving trivial and nontrivial avoided crossings [17,28].

V. DISCUSSION

In any case, the observed BMR sign change implies that the magnetization generated via the direct Edelstein effect, when injecting a given charge current along a device main channel, changes sign as well. Since the BMR depends linearly on the current, our results thus demonstrate a dual control of the BMR (and thus of the current-generated magnetization) by both the current and the gate voltage. This offers interesting possibilities to design alternative spintronic devices. In a H-shaped device such as those sketched in Fig. 4, consisting of two longitudinal arms (left, input and right, output) connected by a transverse arm, applying a charge current in the left arm generates a transverse magnetization able to diffuse as a spin current in the transverse arm over a certain length λ_s in the absence of any net charge displacement. It is then possible to use the IEE at the intersection of the transverse and right arms to convert this spin current back to a charge current whose sign will depend on α_R and on the direction of the spins generated by the EE.

In Fig. 4, we present devices utilizing the direct and inverse Edelstein effects, combined with a gate electric field tuning of the 2DEG band filling, allowing a modulation of the spin-charge interconversion sign and efficiency accordingly. Here, we have demonstrated that the BMR sign can be modulated by a back gate, and for the devices, we propose to use a top gate as it was also shown to efficiently modulate transport properties in STO 2DEGs (see, e.g., Refs. [29,30]) and would be advantageous to integrate and scale down such devices while tuning the required voltages given some adequate material engineering. In Fig. 4(a), a top gate is thus placed at the intersection between the input and transverse arms to modulate the direction of the spins generated by the direct EE. Depending on their direction, the charge current generated by the IEE at the intersection of the transverse and output arms will be positive or negative. Since changing the sign of the charge current in the input arm also reverses the direction of the generated spins and thus of the sign of the output current, we can exploit this dual control to perform logic operations, with the sign of the input charge current J_C^{in} and the sign of the gate voltage V_G as inputs and the sign of the output current as the output. Compiling the different input and output logic states in a truth table shows that this type of device realizes an exclusive-inverted-OR (XNOR) logic function and could be chained with other similar devices.
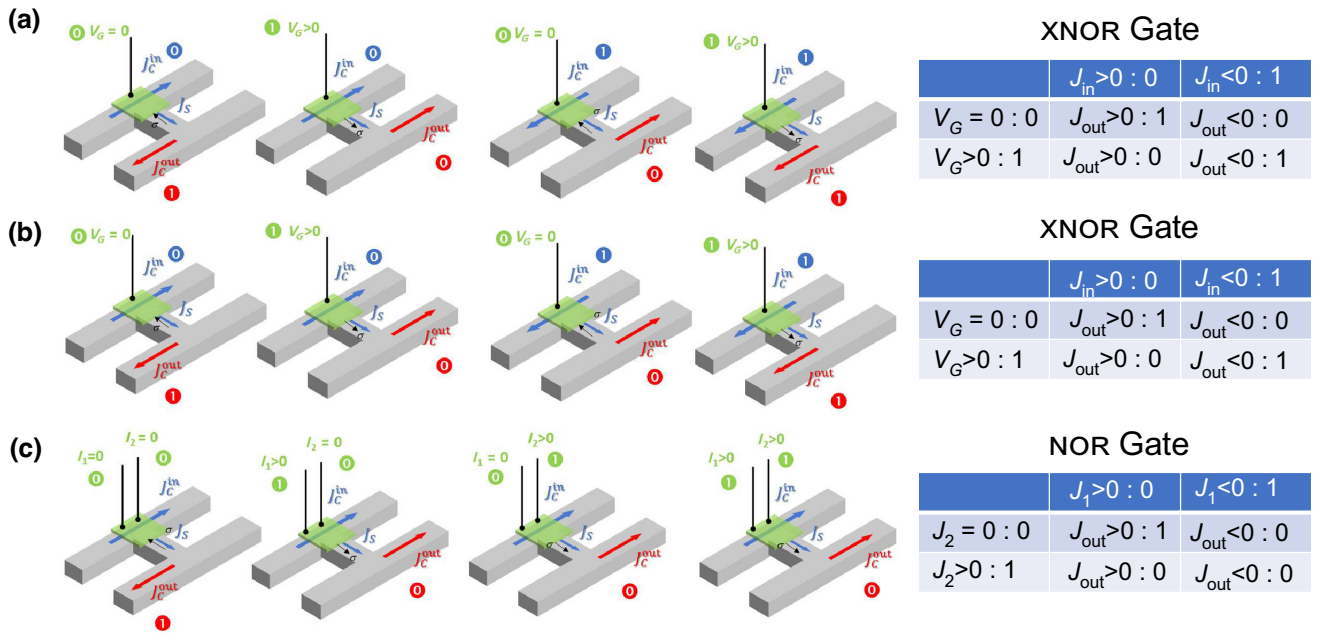
FIG. 4. Examples of three-arm logic gate devices exploiting the direct and inverse Edelstein effects. (a) A gate voltage and the charge-current sign of the first branch are used as inputs, and the sign of the current in the third branch as output, realizing the XNOR logic function. (b) Two independent gate voltages as inputs are applied at the crossing points, with the sign of the current in the third branch as output (XNOR logic gate). (c) Two charge currents are summed together and used as inputs to gate the first crossing, with the sign of the current in the third arm as the output (NOR logic gate).

In Fig. 4(b), a similar logic operation is achieved but now by having two independent top gates, one controlling the sign of charge-spin conversion at the intersection of the input and transverse arms (V_{G1}) and another one controlling the sign of charge-spin conversion at the intersection of the transverse and output arms (V_{G2}). Finally, Fig. 4(c) sketches another device with just one top gate, in which the two inputs are currents I_1 and I_2 accumulating or depleting charges at the top gate. In the absence of any current, the logic gate is in its *high* state as per the truth table in Fig. 4(a). As soon as one of these two currents becomes greater than zero, an effective electric field develops across the gate capacitor, so that the output current of the device J_{out} becomes negative and the logic state becomes zero. The same result is obtained if both currents I_1 and I_2 are above zero, completing the NOR universal logic function.

VI. CONCLUSION

Our work expands the topic of nonreciprocal transport phenomena [31] that is pervading the realm of quantum materials. Nonreciprocal transport has been reported in nonmagnetic topological insulators [11,32], magnetic topological insulators [33,34], noncentrosymmetric superconductors [35], ferroelectric Rashba semiconductors [36], and Rashba interfaces [12–14,16]. While the mechanism may be different depending on the materials systems, the possibility to tune the nonreciprocal transport response by a gate voltage in amplitude *and* sign has been reported in a few systems [32,34], which could ultimately bring the proposed devices to higher operating temperatures. The theoretical efficiency of such devices is discussed in the Supplemental Material (see Ref. [27] for a discussion on the Rashba versus Fermi energies and on the device output-input efficiency—see also Refs. [37–42] therein). This body of results offers exciting possibilities to design spin-orbitronics applications operating at low power, from logic devices such as those proposed here to spin circulators, mixers, isolators, etc., in analogy with nonreciprocal devices operating with photons or magnons [31].

[1] N. Jones, How to stop data centres from gobbling up the world's electricity, Nature **561**, 163 (2018).

[2] B. Dieny, *et al.*, Opportunities and challenges for spintronics in the microelectronics industry, Nat. Electron. **3**, 446 (2020).

[3] J. Sinova, S. O. Valenzuela, J. Wunderlich, C. Back, and T. Jungwirth, Spin Hall effects, Rev. Mod. Phys. **87**, 1213 (2015).

[4] V. Edelstein, Spin polarization of conduction electrons induced by electric current in two-dimensional asymmetric electron systems, Solid State Commun. **73**, 233 (1990).

[5] S. Manipatruni, D. E. Nikonov, C.-C. Lin, T. A. Gosavi, H. Liu, B. Prasad, Y.-L. Huang, E. Bonturim, R. Ramesh, and I. A. Young, Scalable energy-efficient magnetoelectric spin–orbit logic, Nature **565**, 35 (2019).

[6] D. C. Vaz, *et al.*, Voltage-based magnetization switching and reading in magnetoelectric spin-orbit nanodevices, ArXiv:2302.12162 (2023).

[7] P. Noël, F. Trier, L. M. Vicente Arche, J. Bréhin, D. C. Vaz, V. Garcia, S. Fusil, A. Barthélémy, L. Vila, M. Bibes, and J.-P. Attané, Non-volatile electric control of spin–charge conversion in a $SrTiO_3$ Rashba system, Nature **580**, 483 (2020).

[8] M. Fang, Y. Wang, H. Wang, Y. Hou, E. Vetter, Y. Kou, W. Yang, L. Yin, Z. Xiao, Z. Li, L. Jiang, H. N. Lee, S. Zhang, R. Wu, X. Xu, D. Sun, and J. Shen, Tuning the interfacial spin-orbit coupling with ferroelectricity, Nat. Commun. **11**, 2627 (2020).

[9] S. Varotto, *et al.*, Room-temperature ferroelectric switching of spin-to-charge conversion in germanium telluride, Nat. Electron. **4**, 740 (2021).

[10] M. Fiebig, Revival of the magnetoelectric effect, J. Phys. D: Appl. Phys. **38**, R123 (2005).

[11] P. He, S. S.-L. Zhang, D. Zhu, Y. Liu, Y. Wang, J. Yu, G. Vignale, and H. Yang, Bilinear magnetoelectric resistance as a probe of three-dimensional spin texture in topological surface states, Nat. Phys. **14**, 495 (2018).

[12] T. Guillet, C. Zucchetti, Q. Barbedienne, A. Marty, G. Isella, L. Cagnon, C. Vergnaud, H. Jaffrès, N. Reyren, J.-M. George, A. Fert, and M. Jamet, Observation of large unidirectional Rashba magnetoresistance in Ge(111), Phys. Rev. Lett. **124**, 027201 (2020).

[13] D. Choe, M.-J. Jin, S.-I. Kim, H.-J. Choi, J. Jo, I. Oh, J. Park, H. Jin, H. C. Koo, B.-C. Min, S. Hong, H.-W. Lee, S.-H. Baek, and J.-W. Yoo, Gate-tunable giant nonreciprocal charge transport in noncentrosymmetric oxide interfaces, Nat. Commun. **10**, 4510 (2019).

[14] D. C. Vaz, F. Trier, A. Dyrdał, A. Johansson, K. Garcia, A. Barthélémy, I. Mertig, J. Barnaś, A. Fert, and M. Bibes, Determining the Rashba parameter from the bilinear magnetoresistance response in a two-dimensional electron gas, Phys. Rev. Mater. **4**, 071001 (2020).

[15] J. H. Lee, T. Harada, F. Trier, L. Marcano, F. Godel, S. Valencia, A. Tsukazaki, and M. Bibes, Nonreciprocal transport in a Rashba ferromagnet, delafossite $PdCoO_2$, Nano Lett. **21**, 8687 (2021).

[16] L. M. Vicente Arche *et al.* Spin–charge interconversion in $KTaO_3$ 2D electron gases, Adv. Mater. **33**, 2102102 (2021).

[17] D. C. Vaz, *et al.*, Mapping spin–charge conversion to the band structure in a topological oxide two-dimensional electron gas, Nat. Mater. **18**, 1187 (2019).

[18] F. Trier, D. C. Vaz, P. Bruneel, P. Noël, A. Fert, L. Vila, J.-P. Attané, A. Barthélémy, M. Gabay, H. Jaffrès, and M. Bibes, Electric-field control of spin current generation and detection in ferromagnet-free $SrTiO_3$-based nanodevices, Nano Lett. **20**, 395 (2020).

[19] Y. Bychkov and A. E. I. Rashba, Properties of a 2D electron gas with lifted spectral degeneracy, JETP Lett. **39**, 78 (1984).

[20] A. Manchon, H. C. Koo, J. Nitta, S. M. Frolov, and R. A. Duine, New perspectives for Rashba spin–orbit coupling, Nat. Mater. **14**, 871 (2015).

[21] A. D. Caviglia, M. Gabay, S. Gariglio, N. Reyren, C. Cancellieri, and J.-M. Triscone, Tunable Rashba spin-orbit interaction at oxide interfaces, Phys. Rev. Lett. **104**, 126803 (2010).

[22] E. Lesne, Y. Fu, S. Oyarzun, J. C. Rojas-Sánchez, D. C. Vaz, H. Naganuma, and G. Sicoli, Highly efficient and tunable spin-to-charge conversion through Rashba coupling at oxide interfaces, Nat. Mater. **15**, 1261 (2016).

[23] N. Boudjada, I. Khait, and A. Paramekanti, Anisotropic magnetoresistance in multiband systems: Two-dimensional electron gases and polar metals at oxide interfaces, Phys. Rev. B **99**, 195453 (2019).

[24] H. Zhang, X. Yan, X. Zhang, S. Wang, C. Xiong, H. Zhang, S. Qi, J. Zhang, F. Han, N. Wu, B. Liu, Y. Chen, B. Shen, and J. Sun, Unusual electric and optical tuning of $KTaO_3$-based two-dimensional electron gases with 5d orbitals, ACS Nano **13**, 609 (2019).

[25] S. Varotto, A. Johansson, B. Göbel, L. M. Vicente-Arche, S. Mallik, J. Bréhin, R. Salazar, F. Bertran, P. L. Fèvre, N. Bergeal, J. Rault, I. Mertig, and M. Bibes, Direct visualization of Rashba-split bands and spin/orbital-charge interconversion at $KTaO_3$ interfaces, Nat. Commun. **13**, 6165 (2022).

[26] L. M. Vicente-Arche, S. Mallik, M. Cosset-Cheneau, P. Noël, D. C. Vaz, F. Trier, T. A. Gosavi, C.-C. Lin, D. E. Nikonov, I. A. Young, A. Sander, A. Barthélémy, J.-P. Attané, L. Vila, and M. Bibes, Metal/$SrTiO_3$ two-dimensional electron gases for spin-to-charge conversion, Phys. Rev. Mater. **5**, 064005 (2021).

[27] See Supplemental Material at http://link.aps.org/supplemental/10.1103/PhysRevApplied.20.044060. The Supplemental Material contains additional magnetotransport data and a discussion of the signal amplitude and efficiency of the proposed devices.

[28] A. Johansson, B. Göbel, J. Henk, M. Bibes, and I. Mertig, Spin and orbital Edelstein effects in a two-dimensional electron gas: Theory and application to $SrTiO_3$ interfaces, Phys. Rev. Res. **3**, 013275 (2021).

[29] S. Hurand, A. Jouan, C. Feuillet-Palma, G. Singh, J. Biscaras, E. Lesne, N. Reyren, A. Barthélémy, M. Bibes, J. E. Villegas, C. Ulysse, X. Lafosse, M. Pannetier-Lecoeur, S. Caprara, M. Grilli, J. Lesueur, and N. Bergeal, Field-effect control of superconductivity and Rashba spin-orbit coupling in top-gated $LaAlO_3$/$SrTiO_3$ devices, Sci. Rep. **5**, 12751 (2015).

[30] A. Jouan, S. Hurand, G. Singh, E. Lesne, A. Barthélémy, M. Bibes, C. Ulysse, G. Saiz, C. Feuillet-Palma, J. Lesueur, and N. Bergeal, Multiband effects in the superconducting phase diagram of oxide interfaces, Adv. Mater. Interfaces **9**, 2201392 (2022).

[31] Y. Tokura and N. Nagaosa, Nonreciprocal responses from non-centrosymmetric quantum materials, Nat. Commun. **9**, 3740 (2018).

[32] Y. Fu, J. Li, J. Papin, P. Noël, S. Teresi, M. Cosset-Chéneau, C. Grezes, T. Guillet, C. Thomas, Y.-M. Niquet, P. Ballet, T. Meunier, J.-P. Attané, A. Fert, and L. Vila, Bilinear magnetoresistance in HgTe topological insulator: Opposite signs at opposite surfaces demonstrated by gate control, Nano Lett. **22**, 7867 (2022).

[33] K. Yasuda, A. Tsukazaki, R. Yoshimi, K. S. Takahashi, M. Kawasaki, and Y. Tokura, Large unidirectional magnetoresistance in a magnetic topological insulator, Phys. Rev. Lett. **117**, 127202 (2016).

[34] Z. Zhang, N. Wang, N. Cao, A. Wang, X. Zhou, K. Watanabe, T. Taniguchi, B. Yan, and W.-B. Gao, Controlled large non-reciprocal charge transport in an intrinsic magnetic topological insulator $MnBi_2Te_4$, Nat. Commun. **13**, 6191 (2022).

[35] R. Wakatsuki, Y. Saito, S. Hoshino, Y. M. Itahashi, T. Ideue, M. Ezawa, Y. Iwasa, and N. Nagaosa, Nonreciprocal charge transport in noncentrosymmetric superconductors, Sci. Adv. **3**, e1602390 (2017).

[36] Y. Li, Y. Li, P. Li, B. Fang, X. Yang, Y. Wen, D.-X. Zheng, C.-H. Zhang, X. He, A. Manchon, Z.-H. Cheng, and X.-X. Zhang, Nonreciprocal charge transport up to room tempera-

ture in bulk Rashba semiconductor α-GeTe, Nat. Commun. **12**, 540 (2021).

[37] Y. Wang, R. Ramaswamy, M. Motapothula, K. Narayanapillai, D. Zhu, J. Yu, T. Venkatesan, and H. Yang, Room-temperature giant charge-to-spin conversion at the $SrTiO_3$–$LaAlO_3$ oxide interface, Nano Lett. **17**, 7659 (2017).

[38] U. Shashank, A. Deka, C. Ye, S. Gupta, R. Medwal, R. S. Rawat, H. Asada, X. Renshaw Wang, and Y. Fukuma, Room-temperature charge-to-spin conversion from quasi-2D electron gas at $SrTiO_3$-based interfaces, Phys. Status Solidi (RRL) **17**, 2200377 (2023).

[39] J. Varignon, Unexpected antagonism between ferroelectricity and Rashba effects in epitaxially strained $SrTiO_3$, ArXiv:2306.12267 (2023).

[40] A. D. Caviglia, S. Gariglio, N. Reyren, D. Jaccard, T. Schneider, M. Gabay, S. Thiel, G. Hammerl, J. Mannhart, and J.-M. Triscone, Electric field control of the $LaAlO_3$/$SrTiO_3$ interface ground state, Nature **456**, 624 (2008).

[41] A. Joshua, S. Pecker, J. Ruhman, E. Altman, and S. Ilani, A universal critical density underlying the physics of electrons at the $LaAlO_3$/$SrTiO_3$ interface, Nat. Commun. **3**, 1129 (2012).

[42] J. Biscaras, S. Hurand, C. Feuillet-Palma, A. Rastogi, R. C. Budhani, N. Reyren, E. Lesne, J. Lesueur, and N. Bergeal, Limit of the electrostatic doping in two-dimensional electron gases of $LaXO_3$ ($X = Al, Ti$)/$SrTiO_3$, Sci. Rep. **4**, 6788 (2015).